FXS-causing missense mutations disrupt FMRP-containing neuronal granule formation, dynamics, and function

Emily L. Starke[1] and Scott A. Barbee[1,2,*]

[1]Department of Biological Sciences, University of Denver, Denver, Colorado, 80210, USA [2]Molecular and Cellular Biophysics Program, University of Denver, Denver, Colorado, 80210, USA

*Correspondence: scott.barbee@du.edu

SUMMARY

Fragile X Syndrome (FXS) is the most prevalent cause of inherited mental deficiency and is the most common monogenetic cause of autism spectral disorder (ASD). Here, we demonstrate that disease-causing missense mutations in the conserved K homology (KH) RNA binding domains (RBDs) of FMRP cause defects in its ability to form RNA transport granules in both cells and neurons. Using molecular, genetic, and imaging approaches in the *Drosophila* FXS model system, we show that the KH1 and KH2 domains of FMRP regulate distinct aspects of neuronal FMRP granule formation, dynamics, and transport. Furthermore, mutations in both KH domains disrupt translational repression in cells and the localization of known FMRP target mRNAs in neurons. These results suggest that the KH domains play an essential role in neuronal FMRP granule formation and function. Dysregulation of these processes may be linked to FXS.

KEYWORDS

Drosophila, Fragile X Syndrome, FMRP, KH domain, RNA granules, RNA localization, translational regulation, phase separation

INTRODUCTION

Fragile X Syndrome (FXS) is the most common cause of inherited intellectual disability in humans (Santoro et al., 2012). Typically, FXS is caused by epigenetic silencing of the *FMR1* gene due to a long CGG repeat expansion in the 5'UTR, resulting in hypermethylation of the *FMR1* locus and subsequent transcriptional silencing (Pieretti et al., 1991). This results in loss of expression of the encoded Fragile X Mental Retardation Protein (FMRP), an evolutionarily conserved RNA-binding protein that binds to many mRNAs in the mammalian brain. The FMRP protein is best characterized as a translational repressor (Richter and Zhao, 2021). In this role, FMRP associates with diverse ribonucleoprotein particles (RNPs) including RNA transport granules, P-bodies (PBs), and stress granules (SGs) (Lai et al., 2020). In neurons, FMRP-containing RNA transport granules (hereafter called "FMRP granules") are actively transported in both axons and dendrites (Antar et al., 2005; Antar et al., 2006; Dictenberg et al., 2008; Li et al., 2009). These granules carry translationally repressed mRNAs to synapses where they are derepressed in response to synaptic activity. Local translation of critical mRNAs at synapses is essential for long-term synaptic plasticity and is defective in FXS.

In the soma, FMRP binds to translationally repressed target mRNAs and associated RNA-binding proteins (RBPs). These RNPs merge and are remodeled to allow for rapid, motor-dependent transport within neurites (El Fatimy et al., 2016). FMRP granules belong to a diverse class of membraneless organelles (MLOs) that form through liquid-liquid phase separation (LLSP) (Banani et al., 2017). This process is driven by weak, multivalent interactions between protein and RNA components (Mittag and Parker, 2018; Van Treeck and Parker, 2018). Weak interactions allow MLOs to be highly dynamic

and to rapidly assemble and disassemble in response to local signals. In the case of FMRP, posttranslational modification of its C-terminal intrinsically disordered region (IDR) can reversibly control its phase separation *in vitro,* a process that correlates with translational repression (Tsang et al., 2019). This is an attractive model to explain how FMRP granules might assemble, deliver translationally repressed mRNAs to the synapse, and then regulate their local translation in response to activity. However, the role of FMRP in translation and mRNA transport in the context of neurons remains enigmatic.

Although the most common cause of FXS is loss-of-function, advances in gene sequencing have led to the discovery of FXS-causing missense mutations in the *FMR1* gene (Suhl and Warren, 2015). Two mutations are located in conserved N-terminal RBDs of FMRP and have been functionally characterized (De Boulle et al., 1993; Feng et al., 1997; Myrick et al., 2015a; Myrick et al., 2015b; Prieto et al., 2021; Zang et al., 2009). The Gly266Glu (G266E) and Ile304Asn (I304N) mutations are located in K-homology domains (KH1 and KH2 respectively) which bind to "kissing-complex" tertiary motifs or distinct sequence elements (GACR, ACUK, and WGGA) within target mRNAs (Ascano et al., 2012; Darnell et al., 2005; Ray et al., 2013). The latter are ubiquitous sequences in mammalian transcripts (Suhl et al., 2014). Importantly, the analysis of these mutations has also begun to uncover novel functions for *FMR1*. For example, both G266E and I304N disrupt the ability of FMRP to bind to specific target mRNAs and to associate with polysomes suggesting that both KH domains are important for translational regulation (Myrick et al., 2014; Zang et al., 2009). However, the precise role these domains play in FMRP granule formation, dynamics, and function in neurons remains unknown.

Studying FMRP function in mammals is genetically complicated due to the presence of two autosomal paralogs, FXR1P and FXR2P, which have some functional redundancy with FMRP (Agulhon et al., 1999; Wan et al., 2000; Zhang et al., 1995). FMRP interacts with FXR1P and FXR2P within MLOs called "Fragile X granules" with distinct compositions in different regions of the mammalian brain (Akins et al., 2012; Christie et al., 2009; Chyung et al., 2018). In contrast, *Drosophila* has a single *dFmr1* gene and the dFMRP protein shares significant sequence identity with the mammalian protein, particularly within the RBDs (Wan et al., 2000). *Drosophila* FMRP granules are also compositionally similar to those observed in the mammalian brain (Barbee et al., 2006; Cougot et al., 2008). Importantly, *Drosophila* has proven to be an excellent model system in which to study FXS because *dFmr1* mutants recapitulate many FXS phenotypes (Drozd et al., 2018). Here, we have introduced analogous missense mutations into the KH1 and KH2 domains of dFMRP (G269E and I307N respectively) and examined FMRP granules in *Drosophila* Schneider (S2) cells and primary neurons. Our experiments show that wild type FMRP granules that form in neurons are significantly less dynamic than those that form in S2 cells. This is likely to allow these MLOs to resist the shear forces caused by active transport along microtubules in axons and dendrites. Furthermore, the G269E and I307N mutations significantly alter FMRP granule formation, dynamics, and FMRP function in both translational repression and mRNA transport. Collectively, these results provide important insight into the specific neuronal functions of the FMRP protein that are disrupted when *FMR1* expression is lost in cases of FXS.

RESULTS

The KH domains act cooperatively with the IDR to form FMRP granules

The C-terminal IDR of mammalian FMRP is necessary and sufficient to drive the formation of phase-separated liquid droplets *in vitro* (Tsang et al., 2019). However, the dependency of the IDR in FMRP granule formation in cells has yet to be elucidated. To address this question, we first developed a series of dFMRP deletion and mutant constructs (Figure 1A and S1A). Unless otherwise noted, GFP was fused to the N-terminus in order to visualize granules. Importantly, overexpression of a GFP-tagged wild type dFMRP (WT-FMRP) transgene in *Drosophila* larval motor neurons (MNs) replicated published results with untagged dFMRP indicating that the N-terminal GFP tag does not significantly disrupt protein function (Figure S2) (Zhang et al., 2001).

We first transfected *Drosophila* S2R+ cells with WT-dFMRP, dFMRP$_{\Delta IDR}$ (ΔIDR), and dFMRP$_{IDR}$ (IDR) (Figure S1B). As shown previously, 98% of cells transfected with WT-FMRP form numerous small round granules (Figure S1C-F) (Gareau et al., 2013a; Gareau et al., 2013b). The C-terminus of dFMRP is predicted to be disordered, indicating it may play an important role in promoting LLPS (Figure S1A). As with its human ortholog, the IDR alone was sufficient to induce FMRP granules in 65% of transfected cells (Figure S1C-D). These granules were morphologically similar to WT-FMRP although they were significantly less numerous (Figure S1E-F). Interestingly, the structured N-terminal domain of dFMRP (ΔIDR) was also sufficient to induce granule formation in 26% of cells although these granules were less abundant, and many had an amorphic (non-circular) morphology (Figure S1C-F). Based on these observations, we speculated that the KH1 and KH2 domains may contribute to FMRP granule formation. Fusing the KH domains to the IDR (KH+IDR) significantly increased the number of cells containing granules (Figure

S1D). These foci were morphologically indistinct from WT-FMRP granules although the number of KH+IDR granules per cell did not increase significantly (Figure S1C and S1E-F). Collectively, these data indicate that the IDR of dFMRP is sufficient to induce FMRP granule formation in S2R+ cells and that the propensity to form granules is enhanced by addition of the KH domains. However, our data also suggests that additional elements in the N-terminus are likely to be involved in the control of this process.

FXS-causing mutations in the KH domains disrupt granule formation

We next wanted to explore the contribution of each KH domain in FMRP granule formation. The G266E and I304N missense mutations in KH1 and KH2 of hsFMRP are predicted to disrupt the proper folding of each RBD and to disrupt important functions of FMRP including mRNA-binding, AMPA receptor trafficking, and polysome association (Darnell et al., 2005; Myrick et al., 2014; Valverde et al., 2007). To address this, we made analogous point mutations in the KH domains of dFMRP (G269E and I307N), hereafter referred to as KH1* and KH2* (Figure 1A) (Valverde et al. 2007). Next, we transfected S2R+ cells with GFP-tagged constructs to determine the impact these mutations had on FMRP granule formation (Figure 1B). Interestingly, we observed a > 2-fold decrease in the ability of cells expressing GFP-tagged KH1* to form granules relative to WT-FMRP, while KH2* had no effect (Figure 1C-D). This decrease cannot be explained by a difference in the expression levels of GFP-KH1* (Figure 1D). We also found that the number of granules per cell was significantly reduced by both mutations although granules were about twice as abundant in KH2* than KH1* (Figure 1E). Many KH2* granules also had an unusual, often large, amorphic structure while both WT-FMRP and

KH1* granules were generally small and round (Figure 1C and 1F). These results suggest that both the KH1 and KH2 mutants alter normal FMRP granule formation. They also indicate that each KH domain may control a different aspect of this process.

Previous studies have shown that deletion of both KH1 and KH2 from dFMRP causes the formation of large granules in S2 cells (Gareau et al., 2013a; Gareau et al., 2013b). To examine the collective contribution of both domains, we made an identical deletion (ΔKH) and a G269E/I307N double mutant (KH1*KH2*) (Figure 1A). Most cells transfected with these constructs were able to form granules (Figure 1C-D). As with the individual KH mutants, transfected cells contained fewer granules per cell (Figure 1E). Interestingly, most ΔKH and KH1*KH2* granules that formed in cells were large and round indicating that they are different from those containing WT-FMRP, KH1*, or KH2* (Figure 1C and 1F). This also suggests that the KH domains may be involved in regulating the size and shape of FMRP granules. However, we cannot rule out that disruption of both KH domains is significantly changing the overall protein structure and leading to the formation of aggregates containing GFP-ΔKH and GFP-KH1*KH2* protein.

FXS-causing mutations alter the dynamics of FMRP in granules

Previous work has shown that WT-FMRP granules in S2 cells are highly dynamic, with a large fraction of dFMRP capable of rapidly shuttling between FMRP granules and the cytosol (Gareau et al., 2013b). The driving force underlying this process is multivalent interactions between protein and RNA components (Shin and Brangwynne, 2017). To examine dFMRP dynamics in S2R+ cells, we conducted Fluorescence Recovery After Photobleaching (FRAP) experiments. First, we broadly examined the individual roles of

the N- and C-terminal domains (Figure S3A-B). The GFP-tagged IDR, ΔIDR, and KH+IDR constructs each had significantly higher mobile fractions compared to WT-FMRP (Figure S3C). Moreover, the half time of equilibrium ($t_{1/2}$) for each construct was reduced (Figure S3D). Fusion of the KH domains to the C-terminal IDR increased the recovery time by ~ 2-fold but had no impact on the mobile fraction (Figure S3C-D). These data support our conclusion that the IDR and KH domains act cooperatively to stabilize FMRP in granules. Additional elements in the N-terminus are likely further contributing to this process.

We next wanted to determine whether the G269E and I307N mutations had an effect on dFMRP dynamics (Figure 2A-B). In agreement with published results, the fluorescent signal of WT-FMRP recovered to ~ 80% with a $t_{1/2}$ of 21.9s (Figure 2C-D) (Gareau et al., 2013b). The exchangeable pool of dFMRP in both KH1* and KH2* was similar to WT-FMRP (Figure 2C). However, KH1* and KH2* granules recovered rapidly ($t_{1/2}$ = 4.3 and 13.1s respectively) suggesting these foci are much more dynamic than WT-FMRP (Figure 2A-B and 2D). We also examined the effect of removing or disrupting both KH domains on FMRP granule dynamics (Figure 2A-B). The KH1*KH2* mutant significantly reduced the amount dFMRP in the mobile fraction to ~ 66% and rapidly recovered ($t_{1/2}$ = 8.1), similar to that seen with the single mutants (Figure 2C-D). In contrast, the ΔKH mutant substantially increased recovery time ($t_{1/2}$ = 98.7s) (Figure 2D). Together, these data indicate that the G269E and I307N mutations cause the mobile fraction of FMRP granules to be much more dynamic. In contrast, the deletion of both KH domains leads to the stabilization or strengthening of interactions in GFP-ΔKH granules. This further suggests that deletion of both KH domains is causing protein aggregation.

FXS-causing mutations alter the liquid-like properties of stress granules

In addition to neuronal granules (NGs), FMRP is a component of both SGs and PBs in neurons (Lai et al., 2020). We tested whether disease-causing mutations in the KH domains had an effect on the interaction of FMRP with these RNP populations. To examine interactions with SGs, we co-transfected S2R+ cells with the GFP-tagged FMRP constructs and mCherry-tagged Rasputin (Rin), the fly ortholog of G3BP1, a conserved marker for and modulator of SG assembly (Tourriere et al., 2003). In concordance with previous studies, overexpression of Rin induced SG formation in ~20% of unstressed transfected cells (Figure 3A and 3D) (Tourriere et al., 2003). These Rin-positive granules always contained GFP-tagged FMRP and GFP-KH1* always colocalized with Rin (Figure 3A). They were also resistant to treatment with 1,6-hexanediol (1,6-HD), an aliphatic alcohol believed to interfere with weak protein-protein (π-π) and protein-RNA (π-cation) interactions required to form liquid-like MLOs (Kroschwald et al., 2017) (Figure 3D). As expected, arsenite-induced stress triggered the formation of cytoplasmic SGs (Figure 3B). Interestingly, co-transfection with GFP-KH1* or GFP-KH2* significantly reduced the number of cells that formed SGs (Figure 3E). Moreover, SGs that formed in cells co-transfected with all KH mutant constructs were significantly more resistant to 1,6-HD treatment then those transfected with WT-FMRP (Figure 3E). Collectively, this suggests that the liquid-like nature of Rin-positive SGs is partially disrupted by the KH mutations.

Mammalian FMRP shifts its association from polysomes into SGs under conditions of arsenite stress (Kim et al., 2006). In concordance with these results, all GFP-tagged dFMRP constructs colocalized strongly with Rin in arsenite-stressed cells (Figure 3F). As shown previously, this association was reduced in GFP-ΔKH (Gareau et al., 2013b). The

number of cells containing KH1* and KH1*KH2* granules was increased relative to unstressed cells but was still significantly lower than WT-FMRP (Figure 3G-H). As with Rin, all GFP-tagged KH mutants in arsenite-stressed cells were significantly more resistant to 1,6-HD compared to WT-FMRP (Figure 3H). In the case of the KH1* and KH2* mutants, this was not likely due to the persistence of FMRP granules because these nearly disappear in unstressed cells (Figure 3G). This further suggests that the liquid-like nature of arsenite-induced SGs has been disrupted by the single KH mutants. Moreover, the presence of KH1*KH2* and ΔKH granules in unstressed cells provides a third line of evidence suggesting that these mutations are causing FMRP to aggregate.

The KH1 domain is required for the localization of FMRP to P-bodies

In addition to SGs, FMRP has been shown to colocalize with PB proteins in fly and mammalian neurons (Barbee et al., 2006; Cougot et al., 2008). Thus, we were next interested in determining if the KH mutants affected the ability of FMRP to interact with HPat/Pat1p, a highly conserved PB component that colocalizes with FMRP in *Drosophila* neurons (Coller and Parker, 2005; Pradhan et al., 2012). To address this question, we co-transfected S2R+ cells with GFP-tagged FMRP constructs and mCherry-tagged HPat (Figure 3C). As expected, GFP-tagged WT-FMRP overlapped moderately with HPat-positive granules (Figure 3I). In comparison, colocalization was significantly reduced in KH1* and most punctate GFP-KH1* failed to colocalize with punctate HPat (Figure 3C and 3I). Taken together, these data suggest that the KH1 domain is required for the association of FMRP with PBs. In contrast, KH1*KH2* and ΔKH caused the formation of larger granules that strongly colocalized with HPat, suggesting that PB proteins may be

sinking into these structures (Figure 3C and 3I). Based on these results and its propensity to form aggregates, we therefore excluded ΔKH from subsequent analyses.

The KH1 domain is required for FMRP granule formation in primary neurons

FMRP granules are important for the regulated trafficking of FMRP and specific RNA cargos in axons and dendrites (Antar et al., 2004; Antar et al., 2005; Antar et al., 2006; Davidovic et al., 2007; Dictenberg et al., 2008; El Fatimy et al., 2016). Based on our results in S2R+ cells, we asked whether either of the KH domains played a role in the assembly or dynamics of FMRP granules in neurons. Here, we used the φC31 site-directed integrase system to generate transgenic lines carrying an inducible GFP-tagged dFMRP transgene on the third chromosome. First, we examined fly viability in a *dFmr1^{Δ50M}/ dFmr1^{Δ113}* (*Δ50/Δ113*) loss-of-function background when transgenes were expressed in larval motor neurons (*C380-Gal4, cha-Gal80* driver). As previously described, we found that the *Δ50/Δ113* allele combination was viable (Morales et al., 2002). Surprisingly, motor neuron-specific expression of the GFP-KH1* and KH1*KH2* transgenes caused embryonic lethality in *Δ50/Δ113* mutant flies (data not shown). As a result, we conducted all experiments below in a *Δ50/+* heterozygous background.

We next examined FMRP granules in 4-day old primary motor neuron cultures from dissociated larval ventral ganglia. All cells expressing WT-FMRP formed generally small and round granules in the soma (Figure 4A-B). In contrast, only ~ 88% of cells expressing KH2* formed granules and, similar to what we observed in S2R+ cells, they were less numerous and sometimes formed amorphous structures (Figure 4A-B). Strikingly, GFP-KH1* and KH1*KH2* formed few granules in the soma of ~ 2% and 10%

of neurons suggesting that the KH1 domain is required to form FMRP granules *in vivo* (Figure 4A-B). The level of expression of each KH mutant was similar, indicating that this result was not likely due to reduced protein concentrations (Figure 4C). Both WT-FMRP and KH2* granules were also found out in neurites (Figure 4D). However, there were significantly fewer GFP-KH2* granules outside of the soma (Figure 4D-E). Moreover, fewer mutant granules were found in distal regions of neurites (Figure 4F). Together, these data suggest that the KH2 domain is required for FMRP granule transport.

The KH2 domain is important for FMRP granule trafficking in neurites

We next asked if the KH mutations caused defects in the transport of FMRP granules in neurites. As GFP-KH1* and KH1*KH2* do not form granules in neurites (Figure 4A), we focused on *KH2*,Δ50/+* compared to *WT-FMRP,Δ50/+.* Consistent with recent findings of GFP-tagged FMRP in hippocampal neuron dendrites, the majority of WT-FMRP granules were stationary (Figure 4G) (El Fatimy et al., 2016). Although, the number of mobile granules in KH2 mutants was not significantly different, slightly more KH2* granules were transported in the anterograde direction and the velocity of anterograde transport was significantly increased (Figure 4H-J). Despite this increase, total granule displacement was not significantly altered (Figure 4K). While WT-FMRP in neurites was generally round, the shapes of KH2* granules were distorted (Figure 4I). These data, in conjunction with the reduction in the number of FMRP granules found in distal neurites (Figure 4D-F), suggest that KH2 mutant granules have transport defects.

The KH2 domain controls the dynamics of FMRP in neuronal granules

We next performed FRAP analysis in primary *Drosophila* motor neurons, looking at somatic and neuritic granules as two separate populations (Figure 5A-D). In agreement with published results, the mobile fraction of WT-FMRP was significantly lower in both the soma and neurites (33% and 35% respectively) of cultured neurons than in S2R+ cells (82%) suggesting that a larger proportion of WT-FMRP in NGs is found within the non-dynamic fraction (Figure 5E and 2C) (Estes et al., 2008; Gareau et al., 2013b). While the amount found in the immobile fraction of NGs is similar in both compartments, the recovery time of WT-FMRP in the exchangeable pool was about 2-fold slower in neuritic granules ($t_{1/2}$ = 75s) than in those found in the soma ($t_{1/2}$ = 37s) (Figure 5E-F). Additionally, both had slower recovery times than what we saw in S2R+ cells (Figure 2C-D). Together, these data suggest that FMRP granules in neurons are less dynamic than those that form in S2R+ cells. We propose that this increased stability may allow for their active transport along microtubules in neurites without the loss of weakly interacting RNA or protein components. There were two additional observations with KH2* granules that further implicate this mutation in significantly altering FMRP granules. First, the amount of KH2* found in the mobile fraction was significantly smaller in both somatic and neuritic NGs (Figure 5E). Second, the recovery time of KH2* was significantly reduced ($t_{1/2}$ = 5s) in both compartments relative to controls (Figure 5F). These data indicate that the composition and dynamics of FMRP granules have been altered by the KH2 mutation which may be contributing to the transport defects seen in KH2* granules (Figure 4).

The KH domains are essential for the translational repression activity of FMRP

We next wanted to examine the role of the KH domains in regulating the translational repression activity of dFMRP. Both KH1* and KH2* have been shown to disrupt the association of FMRP with polysomes suggesting that both KH domains are important for translational repression (Darnell et al., 2005; Feng et al., 1997; Myrick et al., 2014; Zang et al., 2009). Moreover, the KH domains of dFMRP regulate translation by binding directly to the 80S ribosome to block elongation (Chen et al., 2014). To examine the role of the KH domains in regulating mRNA translation, we modified a λN-based tethering assay in S2 cells, where the 3'UTRs of known dFMRP target mRNAs were fused to the 3' end of a firefly luciferase reporter, or FLuc (Figure 6A) (Rehwinkel et al., 2005). In order to eliminate RNA binding as a mechanism, we first tethered λN-tagged FMRP constructs directly to the reporter via a 5X tandem BoxB sequence in the SV40 3'UTR. WT-FMRP and KH2* constructs were both able to repress translation (Figure 6B). In contrast, the ability of KH1* to repress reporter expression was significantly disrupted, suggesting that the KH1 domain is required to regulate repression activity. These data are consistent with an earlier study using a different, non-disease associated KH1 mutant (I244N) and a reporter in an *in vitro* translation system (Chen et al., 2014).

Next, we were interested in addressing whether untethered dFMRP could translationally repress Fluc by binding to the 3'UTRs of known mRNA targets and if either of the KH domains were required for this to occur. To examine this, we replaced the 3'UTR containing the BoxB repeats with the 3'UTRs from mRNAs encoding for: 1) the degenerin/epithelial sodium channel (DEG/ENaC) family member, *pickpocket* (*ppk*); 2) the Ca^{2+}/calmodulin-dependent protein kinase II, *camkii*; 3) the profilin ortholog, *chickadee (chic)*; and 4) its own mRNA, *fmr1* (Reeve et al., 2005; Sudhakaran et al., 2014;

Xu et al., 2004; Zhang et al., 2001) (Figure 6A). As with the BoxB reporter, the KH1 domain was required to regulate repression of the *ppk*, *chic*, and *fmr1* reporters as repression was ameliorated in KH1* and KH1*KH2* (Figure 6B-E). The efficiency of repression of each of these reporters by WT-FMRP and KH2* is variable, likely due to differences in the ability of these proteins to interact with the 3'UTR. In contrast, the *camkii* reporter was different in that repression is slightly but significantly derepressed by both KH2* and KH1*KH2* indicating that the KH2 domain is required for repression (Figure 6F). Collectively, these data indicate that FXS-causing mutations in the KH1 and KH2 domains differentially disrupt translational repression. Derepression of translation in KH1* correlates with defects in its ability to form FMRP granules in S2 cells (Figure 1C-D).

The KH domains are required for the transport of FMRP target RNAs

NGs are a specialized type of MLO within neurons that serve to transport translationally silent mRNAs between the soma and axonal or dendritic compartments (Formicola et al., 2019). As we have shown that the KH domains are essential in providing distinct mechanisms for forming FMRP granules and regulating their dynamics, we next asked if *KH1*,Δ50/+* and *KH2*,Δ50/+* neurons had defects in target mRNA localization. To address this question, we used single-molecule fluorescence *in situ* hybridization (smFISH) to quantify the number of transcripts in the soma and neurites of primary motor neurons. We focused on two known mRNA targets of dFMRP in flies, *camkii* and *chic*, both of which interact with dFMRP-containing NGs in primary motor neurons (Barbee et al., 2006; Estes et al., 2008). We find that there are significantly more *camkii* transcripts in *WT-FMRP,Δ50/+* neurites compared to *GFP,Δ50/+* controls suggesting that dFMRP

promotes the transport of the *camkii* mRNA (Figure 6G and 6I). In neurons expressing either KH1* or KH2*, *camkii* transcripts are not significantly reduced in neurites compared to *WT-FMRP,Δ50/+* controls (Figure 6I). Different results were observed using smFISH probes targeting *chic* (Figure 6H and 6J). The percentage of transcripts in KH1* and KH2* neurites was significantly reduced compared to *WT-FMRP,Δ50/+* neurons (Figure 6I). Collectively, these data suggest that the KH1 and KH2 domains are differentially required to regulate the trafficking of *camkii* and *chic* mRNAs in neurites of cultured neurons. This correlates, in part, with the disruption of FMRP granule formation and dynamics.

DISCUSSION

We provide multiple lines of evidence indicating that the KH domains of FMRP are differentially required to regulate FMRP granule assembly, dynamics, and function in neurons. First, an FXS-causing missense mutation in the KH1 domain disrupts the ability of FMRP to form granules in primary neuron cell culture (Figure 4A-B). In contrast, KH2 mutants form granules in the soma but their transport to distal neurites is disrupted (Figure 4D-F). Second, WT-FMRP granules in neurons contain a larger immobile fraction ("stable core") and smaller mobile fraction ("dynamic shell") as assessed by FRAP (Figure 5). This core/shell architecture is consistent with other RNPs such as SGs (Jain et al., 2016). We find that KH2* significantly increases the core/shell ratio and decreases the stability of FMRP in the dynamic shell (Figure 5E-F). Third, the KH1 domain is required to regulate the translation of reporters for known target mRNAs (Figure 6B-F). Finally, both the KH1 and KH2 domains are required to localize specific target mRNAs to neurites (Figure 6G-

J). Translational repression and RNA transport are processes that have been directly attributed to FMRP-containing RNA granules in neurons (Richter and Zhao, 2021).

Multivalent interactions drive FMRP granule formation in cells

The disordered C-terminus of mammalian FMRP is necessary and sufficient to drive the formation of phase-separated droplets *in vitro* (Tsang et al., 2019). Furthermore, serine/threonine phosphorylation patterns of amino acids in this region control the propensity to phase separate with RNA and regulate rates of deadenylation and translation within these condensates (Kim et al., 2019). Collectively, these data suggest that regulation of FMRP phase separation may serve as a simple mechanism to allow for the delivery of translationally repressed mRNAs to synapses and their local translation in response to activity. Through our analysis of *Drosophila* FMRP granules cells *in vivo*, we show that the C-terminal IDR is sufficient to regulate granule formation (Figure S1). However, formation of morphologically and biophysically "normal" FMRP granules requires the cooperative interaction with interacting domains found within the structured N-terminus including the KH motifs (Figure S1 and S3). This is consistent with published results (Gareau et al., 2013a). RNA granule formation is driven by LLPS wherein molecules reach a critical concentration and spontaneously form a condensate (Alberti, 2017). While IDRs often play a major role, multivalent interactions between components are often the driving force for this process by providing a scaffold of cis-acting binding sites that allow for interactions with multiple trans-acting protein or RNA species (Mittag and Parker, 2018; Van Treeck and Parker, 2018). These binding partners are often also capable of interacting with other proteins or RNAs, thus allowing these molecules to

concentrate and compartmentalize within the cell (Banani et al., 2016; Li et al., 2012). Our results support the model where multivalency is playing a significant role in the ability of FMRP to form RNA transport granules (Martin and Holehouse, 2020). It is important to note that our *in vivo* studies are not able to differentiate whether FMRP is seeding the formation of a *de novo* MLO or if it's being recruited to a pre-formed NG (SG, PB, etc.).

Neuronal FMRP granules are inherently stable structures

NGs and other types of RNA transport granules are unique MLOs because they are actively transported through the cytoplasm through an association with molecular motor proteins. If NGs are liquid-like and not delimited by a membrane, how do they move rapidly through the cytoplasm without the loss of their constituent molecules? Analysis of TDP-43 RNP granules in axons of rodent primary cortical neurons shows that these NGs are generally round at rest and their shape deforms under the shear stress induced by active transport (Gopal et al., 2017). The shape, density, and biophysical properties of these granules differs between proximal and distal TDP-43 RNPs with those located in regions closer to the cell body being much less dynamic (Gopal et al., 2017). However, NG populations are heterogenous and the mobile fraction and recovery times as determined by FRAP vary significantly (Chae et al., 2010; Cougot et al., 2008; Formicola et al., 2019; Gopal et al., 2017; Vijayakumar et al., 2019). We find that WT-FMRP granules are less dynamic in *Drosophila* primary motor neurons than in S2R+ cells (Figure 2 and 5). These data are consistent with differences in the dynamics of dendrite-localized neuronal P-body components in rodent primary hypothalamic neurons and HeLa cells (Cougot et al., 2008). Also consistent with our results, mammalian and fly neuronal FMRP

granules in neurites have been shown to be stable structures with most FMRP residing within the non-dynamic core and with longer recovery rates (Figure 5) (Antar et al., 2005; Estes et al., 2008). Thus, neuronal FMRP granules are likely to be examples of metastable condensates with solid-like characteristics. We predict that this compact and non-dynamic structure helps efficiently facilitate their transport in neurons.

The KH domains differentially regulate FMRP granule formation and dynamics

Disease-causing missense mutations in FMRP have allowed for the isolation of specific functions of FMRP that are contributing to the pathogenesis of FXS (Suhl and Warren, 2015). We show that, while mutations in the KH1 and KH2 domains both impact FMRP granule formation, KH1* phenotypes are significantly stronger. This is supported by three lines of evidence. First, granule formation in KH1* is significantly diminished in S2R+ cells and nearly eliminated in neurons (Figure 1 and 4). Second, KH1* has a greater effect on FMRP granule dynamics (Figure 2). Finally, KH1* has a stronger effect on the association of FMRP with both SGs and PBs in S2R+ cells (Figure 3). Why does the KH1 mutation have a more significant impact on FMRP granules? While the precise RNA binding sites are a source of debate, it is clear that the KH domains of FMRP bind with different specificity and/or affinity to target mRNAs (Athar and Joseph, 2020). Interactions occurring via the KH1 domain could be shifting the concentration threshold required to promote FMRP granule formation. RNA has been implicated in promoting LLPS in FMRP and in other proteins such as hnRNPA1 and FUS, by shifting the phase boundary and requiring lower protein concentrations to initiate demixing (Molliex et al., 2015; Schwartz et al., 2013; Tsang et al., 2019). It is possible that the KH1 domain is

contributing disproportionately strong (or numerous) interactions with specific neuronal RNA targets which is shifting the critical concentration needed for granule formation.

FMRP has also been shown to interact with polysomes and experiments indicate that the KH domains of dFMRP interact directly with the peptidyl site (Chen et al., 2014). This suggests a mechanism by which FMRP stalls translational elongation by sterically inhibiting tRNA entry. The non-disease associated KH1 mutant (I244N) and KH2* (I307N) both disrupt binding affinity with the I244N mutation having a stronger effect (Chen et al., 2014). Interestingly, analysis of FMRP granules in mouse brain homogenates by electron microscopy found that FMRP and ribosomes both localize to a subset of neuronal RNA transport granules (El Fatimy et al., 2016). These data led the authors to propose that FMRP granules form in the soma from stalled polysomes. A prediction from this model is that disruption of the FMRP-ribosome association would negatively impact FMRP granule formation as it represents an additional, and potentially essential, multivalent interaction. This model is consistent with our data showing that KH1* and KH2* both disrupt FMRP granules, with the KH1 mutant having a stronger effect (Figure 1 and 4).

The relationship between FMRP granule formation and function

A role for the KH1 domain in regulating both translational repression and FMRP granule formation sheds light on the relationship between these two processes. We demonstrate that FMRP can repress the translation via the 3'UTRs of known target mRNAs and that the translation of all but *camkii* is derepressed by the KH1 mutation (Figure 6A-F). The derepression we observe in KH1* is consistent with observations that this mutation has a significant impact on the affinity of dFMRP for the ribosome (Chen et

al., 2014). If stalled polysomes are the basic unit for FMRP granules, then it is perhaps not surprising that KH1* disrupts FMRP granule formation. Therefore, our data suggests that FMRP granule formation is likely a consequence of translational repression.

FMRP granules are also linked to the transport of mRNAs in axons and dendrites (Antar et al., 2005; Antar et al., 2006; Dictenberg et al., 2008; Li et al., 2009). We demonstrate that FMRP can promote the localization of two target mRNAs to distal neurites in primary cultured neurons (Figure 6G-J). Localization of *chic* is disrupted by KH1* and KH2* suggesting that both domains are required to regulate this transcript. Differences between the requirement for these domains for *camkii* and *chic* localization may be reflective of differences between these transcripts. It has been hypothesized that each neuronal RNA granule contains and transports a single RNA (Schuman et al., 2006). Based on this, it is likely that *camkii* and *chic* are transported in different RNPs.

Conclusions

The role of FMRP granules in the transport and translation of target mRNAs in neurons is complex because their organization, dynamics and function are regulated by multivalent interactions involving structured and unstructured protein domains. Our data supports a model where FMRP granules are solid-like metastable MLOs, a state that is necessary to allow for their active transport in neurites without the loss of components. FXS-causing missense mutations in FMRP are interesting in the sense that they do not cause FMRP to form pathological inclusions in cells. This is distinctly different from disease-causing mutations in numerous IDR-containing RBPs that have been linked to neurodegenerative disease such as TDP-43, FUS, or hnRNP-A1 (Molliex et al., 2015;

Patel et al., 2015). In contrast, forming metastable structures appears to be a primary function of FMRP granules in translational repression and RNA transport in neurons.

METHODS

Fly stocks and husbandry

In all experiments, both male and female flies were used. All lines were incubated at 25°C with 12-hour light/dark cycles and 60% humidity on standard Bloomington medium. Fly lines used and made in this study are listed in Key Resource Table.

pUAST:attB:EGFP flies were generated via restriction cloning *EGFP* and each *EGFP-FMRP* mutant into the multiple cloning site of *pUAST-attB* for directional cloning via the 5'-*KpnI* and 3'-*XbaI* cloning sites. *pUAST:attB:EGFP* and *pUAST:attB:EGFP-FMRP* mutants were sent to *BestGene* for injection into fly strain #24485 for *PhiC31* integration into chromosome III. *pUAST:attB:EGFP-FMRP* mutant flies were recombined with w^{1118};; $FMR1^{\Delta 50M}$/TM6B, Tb^+,$FMR1^+$ mutant flies for FMRP primary motor neuron experiments. Recombinants were genotyped for the $FMR1^{\Delta 50M}$ deletion by knocking out a single adult in a PCR tube on ice for 5 minutes. Flies were squished with a 200 μL pipette tip in 5μL of squishing buffer (10 mM Tris-Cl pH 8.0, 1 mM EDTA, 25 mM NaCl, and 0.2 mg/mL proteinase K) and incubated at room temperature for 20 minutes. Samples were then boiled at 95°C for 5 minutes, cooled on ice for 3 minutes and spun down at 16,000X G for 5 minutes in benchtop centrifuge. For genotyping, 5 μL of the supernatant (genomic DNA prep) was used in a standard NEB One Taq Polymerase PCR reaction using the *FMR1* deletion forward and reverse primers which were annealed at 60°C and elongated for 7 minutes as described by Zhang et al. (Zhang et al., 2001). PCR products

were ran in a 1% agarose gel following standard DNA gel electrophoresis procedures and probed for the presence of a 4.2 kbp (deletion) or 6.8 kbp (*wildtype*) PCR product.

Schneider's S2R+ and S2 cell culture

S2 and S2R+ cells were maintained at 24°C with ambient humidity in a dark incubator and maintained on Shields and Sang M3 media (Sigma-Aldrich; S8398) containing bactopeptone and yeast extract, and supplemented with 10% fetal bovine serum (Gibco; 16000044), 1% penstrep (Invitrogen; 15070-063) and fungizone (Invitrogen; 15290-026), also known as M3+BPYE media. DNA transfections were performed with Qiagen's Effectene Transfection Reagent kit (Qiagen; 301425) (see below). Most experiments were conducted on S2R+ cells due to their higher propensity to adhere to and flatten out on cover slips, making imaging stationary cells more reliable.

***Drosophila* third-instar primary larval motor neuron tissue culture**

Primary motor neurons were cultured from wandering 3rd instar larvae using a tissue culture protocol adapted from Barbee et al. 2006. For each genotype, 10 larvae were washed briefly in 70% ethanol, followed by five one-minute washes in 1xPBS pH 7.4. CNS's were dissected from 3rd instar larvae in supplemented media, or M3+BPYE media supplemented with 50 µg/mL insulin (Sigma-Aldrich; I6634), from which optic lobes were also removed leaving only the ventral ganglia (VG). VG were washed briefly in supplemented media five times and then transferred to a sterile microfuge tube containing ~1 mL of Rinaldini's solution (800mg NaCl, 20mg KCl, 5mg NaH2PO4*H2O, 100mg NaHCO3, 100mg glucose, and 1mL penstrep to final volume of 100 mL). VG were spun

for 5 minutes at 3,000 RPM. Supernatant was carefully removed and fresh Rinaldini's solution was added, vortexed, spun down and removed a total of five times to wash off residue yeast and other contaminants. In a sterile hood supernatant was removed and 1mL of Liberase (Roche; LIBDH-RO; containing collagenase and dispase) supplemented Rinaldini solution was incubated with VG for 1 hour. The dissociated tissue was then spun down for 5 minutes at 3,000 RPM. Supernatant was discarded and VG were washed another 4 times with supplemented M3+BPYE media. Following this, the supernatant was removed and VG were resuspended in 200µl of supplemented media. The dissociated VG were titrated with a fire-polished, glass Pasteur pipette 56 times and then 175 times with a medium coated P200 tip. The MN cell suspension was then seeded onto a single Concanavalin-A (Sigma-Aldrich; C2010) and Laminin (Corning; CB-40232) coated #1 or #1.5 35mm glass bottom dish (Cellvis; D35-10-1-N). Once plated, cells were incubated at 24°C with ambient humidity in a dark incubator 3-5 days before imaging. Media was carefully aspirated and replaced every other day until imaged.

Molecular cloning and Site directed mutagenesis

FMR1-RD cDNA obtained from DGRC was PCR amplified and cloned into the multiple cloning site of the pAcB5.1-EGFP vector using the 5'-HindIII and 3'-EcoRI restriction sites to make pAcB5.1-EGFP-FMRP. For S2R+ cell fluorescence imaging, pAc5.1B:EGFP-FMRP-IDR and ΔKH mutants were cloned into the multiple cloning site of pAc5.1B-EGFP following PCR amplification from the target ORFs from pAc5.1B:EGFP-FMRP. Amplification primer sequences and sites are listed and described in the Key Resource Table. The human KH1 Gly266Glu and KH2 Ile304Asn point mutations are

orthologous to *Drosophila* Gly269Glu and Ile307Asn, respectively. To generate these FXS-causing point mutants in *Drosophila* FMRP, SDM primers were designed using the "substitution" feature in NEBaseChanger v1.2.9 (New England BioLabs Inc.). Mutagenesis was designed to occur at nucleotide 805-807 (GGA→ GAA) and nucleotide 868-870 (ATC→ AAC) in the KH1 and KH2 domain, respectively. NEB's Q5 Site-Directed Mutagenesis Kit Protocol (E0554) was conducted on the *pAc5.1B:EGFP-FMRP* vector to introduce the KH1 and KH2 missense mutations. The following modifications were made to NEB's mutagenesis PCR reaction: KH1 mutagenic primers Ta=62℃, elongation at 72℃ for 4 minutes; KH2 mutagenic primers Ta= 64℃, elongation at 72℃ for 4 minutes.

To clone the SG protein, Rasputin, into a C-terminally tagged mCherry vector, we constructed a $(Gly_4Ser)_3$ linker-mCherry pAc5.1 vector. The mCherry-tag was amplified from *pAc5.1B-mCherry* which included 5'-*HindIII* and 3'-*BamHI* restriction sites for directional cloning into *pAc5.1B* with an in-frame stop codon following the mCherry sequence. Primers for cloning the $(Gly_4Ser)_3$ linker upstream of mCherry were also designed to allow for ligation of the three fragments (pAc5.1 + $(Gly_4Ser)_3$ + mCherry) in the correct orientation. To amplify Rasputin (Rin) to clone into the mCherry vector, total RNA was extracted from four BL Canton S adult males using the Zymogen RNA extraction kit and following the manufacturer's protocol (Zymo Research Corporation; R2060). RT-PCR was then conducted on total RNA using Clontech's RNA to cDNA EcoDry™ Premix (Oligo dT) kit (#639543). Rasputin cDNA was amplified using primers that added 5'-*HindIII* and 3'-*EcoRI* restriction sites for directional cloning into the mCherry vector to make the final *pAc5.1B:Rasputin-(Gly₄Ser)₃-mCherry* vector.

The firefly luciferase, or FLuc reporters, used in the translation reporter assays were all sourced from the *pAc5.1C:FLuc:Stop:5BoxB* backbone vector (Addgene #21301). The 5BoxB 3'UTR was replaced with the 3'UTRs of *FMR1* and *camkii* by restriction or Gibson cloning methods. We cloned the *camkii* isoform with the long 3'UTR, so that all possible binding sites were conserved in the reporter. DNA from 4 adult male BL Canton S flies was extracted and purified using the E.Z.N.A Tissue DNA kit (Omega Bio-Tek #D3396-01). From the extracted DNA, the long 3'UTR of *camkii* was amplified using the *CaMKIIUTRFwdGA* and *CaMKIIUTRRvsGA* primer set, then purified using Zymogen's DNA Clean and Concentrator-5 Kit (#11-302C). *pAc5.1C:FLuc:Stop:5BoxB* was digested with *EcoRI*-HF and *XhoI* following NEB's general protocol for restriction enzymes to remove the 5xBoxB 3'UTR. The *camkii* 3'UTR was then cloned into the luciferase destination vector via Gibson Assembly (#E2611) following NEB's protocol. The *FMR1* 3'UTR was similarly amplified using the FMR1Fwd and FMR1Rvs primer set and then cloned into the *pAc5.1C:FLuc:Stop:5BoxB* destination vector using the 5'*EcoRI* and 3'*XhoI* restriction sites while removing the 5xBoxB sequence.

S2R+ and S2 cells transient transfections and cell viability assay

Transient transfections were performed following Qiagen's standard Effectene reagent protocol in which 0.5 µg of each construct was optimized, except for *pAc5.1B-EGFP:FMRP:KH1** in which 0.75 µg was transfected per 1 million cells in a 12-well plate. Transfected cells were grown for approximately 72 hours before used in assays.

Live cell imaging and analysis of granule

For granule formation, morphology and count assays, live cell imaging was conducted on transiently transfected S2R+ cells. Cells were plated on poly-d lysine coated imaging dishes 72 hours post-transfection and imaged within 2 hours of plating. In all experiments, images were obtained using an Olympus FV3000 confocal laser scanning microscope and cells were visualized with a 100x (NA 1.4) objective digitally zoomed to 2.95x for best resolution.

To count the number of transfected cells able to form granules, approximately 100 cells were manually identified at the microscope. The total number of cells that formed granules out of all EGFP-expressing cells were counted. Cells were scanned through in z to make sure that granules in any plane were identified. The number of granule forming cells was divided by total number of transfected cells in three separate experiments.

To compare the propensity of the different mutants to form circular granules, approximately 100 granule forming transfected cells were identified at the microscope. The number of cells forming circular and amorphic (non-circular) granules were counted. In most cases, cells that formed amorphous granules also contained circular granules, however, cells that formed any number of amorphous granules were categorized as amorphic.

Finally, to count granules formed by each FMRP-mutant, 15 cells were analyzed in a single experiment. The z-plane where the nucleus took up the largest cell area was examined. Punctate areas of fluorescence intensity above background were considered to be granules and counted using ImageJ's cell counter plugin. For each image, both cell diameter (through the longest axis in the same z-plane) and granule number were collected. From this, the number of granules per cell area (μm^2) was plotted.

Data from each of these experiments was entered into Excel for initial analysis.

These data were then entered into Prism for statistical analysis.

Fluorescence Recovery After Photobleaching

For FRAP experiments, 17-21 EGFP positive granules were viewed with a 100x

(NA 1.4) objective digitally zoomed to 2.95x and photobleached with the lowest laser

intensity necessary to completely bleach ROI, ranging from 2.44-10% 488nm laser power

for 500-1,000 milliseconds. Two pre-FRAP images were collected and images were

captured every 1.0878 seconds pre and post bleaching for a total of 200 frames.

To set up the FRAP analysis, images were initially processed in ImageJ2/FIJI

(Rueden et al., 2017; Schindelin et al., 2012). Data were analyzed essentially as

described in (Cheney et al., 2017). A ROI was manually traced in each FRAP movie for

1) the bleached granule, 2) an unbleached granule and 3) diffuse cytoplasmic staining for

background. To ensure that fluorescence was accurately measured the ROI was moved

throughout the movie if/when granules moved in x/y out of the initially set ROI to maintain

consistency. From these movies, the mean fluorescent intensity was obtained for each

frame and plugged into an excel sheet. Using these data, the following was calculated:

1) Photobleach Correction Value (PCV), in which the initial pre-bleach unbleached

granule average fluorescence intensity was divided by each subsequent unbleached

granule average intensity, 2) Corrected Average Intensity (CAI), where the bleached

granules mean intensity was multiplied by the PCV, 3) Background Corrected

Fluorescence Intensity (BCFI), where the CAI was subtracted by the average intensity of

the background ROI, and 4) the Final Corrected Value (FCV) which was calculated by

dividing each BCFI by the initial BCFI value and multiplying by 100 to get a normalized fluorescence intensity profile. The FCV's from each movie were then plugged into a one-phase association, nonlinear fit in Prism to calculate the fluorescence recovery curve, mobile fraction, and half-life.

Immunocytochemistry, arsenite and 1,6-hexanediol treatments

The following immunocytochemistry procedure was followed for all S2R+/S2 cell imaging, unless indicated otherwise. Cells were plated, immunostained and imaged on 35 mm glass bottom dishes with 10mm #1 cover glass (Cellvis; D35-10-1-N). After allowing cells to settle on imaging dishes for at least 20 minutes, they were fixed with 4% PFA for 10 minutes followed by a 5-minute incubation with ice cold methanol at -20°C. Cells were washed three times for 5 minutes in 1xPBS (pH 7.4), permeabilized in 1xPBST (pH 7.4) for 10 minutes, and then blocked in 1xPBST with 2% BSA (w/v; Sigma-Aldrich, A9647) and 5% normal goat serum (v/v; Sigma-Aldrich, S26-M) for 30 minutes. Cells were incubated with primary antibodies overnight at 4°C, washed in 1xPBS, and then incubated for 1 hour in secondary antibodies at room temperature. Cells were washed with 1xPBS and then mounted in DAPI-Fluoromount-G Clear Mounting Media and sealed by adhering a #1 coverslip to the dish.

For FXS-causing point mutants and HPat colocalization experiments, immunostaining was conducted on cells transfected with *pAc5.1B:EGFP-FMRP* and FXS-causing point mutants. For this assay, rabbit anti-HPat (1:1,500) primary and goat anti-rabbit Alexa-567 (1:500) secondary antibodies were used.

To induce stress, cells were co-transfected with *pAc5.1B:EGFP-FMRP* mutants and *pAc5.1B-Rasputin(Gly₄Ser)₃mCherry*. At 72 hours post transfection, cells were treated with 0.5mM sodium meta-arsenite in M3+BPYE media for 45 minutes. For colocalization analysis, cells were immediately fixed in 4% PFA for 10 minutes, incubated with ice cold methanol at -20°C for 5 minutes and then washed 3 times for 5 minutes in 1xPBS (pH 7.4). Preparations were then mounted in DAPI-Fluoromount-G Clear Mounting Media (Southern Biotech).

For analysis of granules with 1,6-hexanediol, cells were co-transfected with *pAc5.1:EGFP-FMRP* mutants and *pAc5.1-Rasputin(Gly₄Ser)₃mCherry*. Non-stressed cells were imaged via CLSM on either fresh cell culture media or 10% 1,6-HD (w/v) in media. Cells were imaged within 20 minutes of the addition of 1,6-HD as cells start to bleb and stress granules begin to form after long exposure times (Wheeler et al., 2016). Stressed cells were treated with 0.5 mM sodium arsenite for 45 minutes before the addition of fresh 0.5 mM arsenite, or 0.5 mM arsenite + 10% 1,6-HD. In all conditions, approximately 100 live transfected cells were analyzed for the presence of FMRP or Rin granules, in triplicate. Data from each of these experiments was entered into Excel for initial analysis. These data were then entered into Prism where we performed statistical analysis and created graphs.

Colocalization analysis

To determine the degree to which FMRP mutants colocalized with SG or PB components, 12-13 images were analyzed in ImageJ/FIJI using the Just Another Colocalisation Plugin, JACoP (Bolte and Cordelières, 2006). In all cases, images were

cropped to the smallest area possible to eliminate colocalization events outside of the cell of interest and images for FMRP/HPat colocalization were background subtracted to a rolling ball radius of 50 pixels to account for the higher degree of HPat background staining. In JACoP, Pearson's coefficient analysis was performed between the FMRP and SG or PB channels which were recorded in Excel and analyzed in Prism.

Western blotting

Western blots were generally carried out as follows. Samples were boiled at 95°C for 10 minutes, chilled on ice for 5 minutes and sonicated for three one second pulses, with one second pauses in between at 50 mW on ice. Samples were chilled on ice for 5 minutes before clarification at 15,000X G for 15 minutes at 4°C. Supernatants were carefully transferred to a fresh microfuge tube on ice, and then 15-25 µL of sample was added per well in a 4-20% Mini-PROTEAN TGX Precast Protein Gel (Bio-Rad, #4561094). Gels were run at 250V for 35 minutes or until adequate separation was achieved. Prior to protein transfer, the SDS-PAGE gel and nitrocellulose membrane were equilibrated in 1x transfer buffer for 10 minutes with agitation. Gel transfer to nitrocellulose membrane was run at 120V for 45 minutes on a stir plate with an ice pack to keep the solution cool. The nitrocellulose membrane was then incubated in blocking solution (5% non-fat milk in 1X TBST pH 7.4) for 30 minutes at room temperature with agitation. Primary antibodies were diluted in blocking solution (5% nonfat milk in 1x TBST pH 7.4) and incubated with membrane for either 2 hours at room temperature or overnight at 4°C with agitation. Membranes were washed 5 times in 1X TBST with agitation. Secondary antibodies were diluted in blocking solution and incubated with membrane for

45 minutes to 1 hour at room temperature with agitation. Membranes were washed in TBST for 5 minutes 3 times with agitation. Approximately 1 mL of Thermo Scientific SuperSignal West Dura Chemiluminescent Substrate (Thermo Scientific; 34075) was incubated with membrane before imaging on a FluorChem R (ProteinSimple).

For westerns conducted on *EGFP-FMRP* mutant ectopic expression assays in S2R+ cells, transfected cells were harvested at three days post-transection from a 6-well plate. Cells were scraped and resuspended by pipetting up and down and 1.5 mL of cells were spun down at 1,000x G for 5 minutes at 4°C. Cells were then resuspended in 400 μL of 2x Laemmli sample buffer + **β**-mercaptoethanol on ice.

For westerns conducted on C380, cha-Gal80/+ ; ; UAS:EGFP-FMRP, FMR1^{Δ50M}/+ larvae ectopically expressing the FXS-causing point mutants, 5 CNS's were diluted in 100μL of 2x Laemmli sample buffer + **β**-mercaptoethanol on ice. CNS's were homogenized in a 1.6 mL microcentrifuge tube for 30 seconds on ice using a hand-held homogenizer. Homogenate was incubated on ice for 3 minutes, and then processed as indicated above.

For both of these assays, the primary antibodies used were mouse anti-*dFMR1* (1:3,000), rabbit anti-*EGFP* (1:2,000), and mouse anti-*α-tubulin* (1:1,000). Secondary antibodies used were horse anti-mouse HRP or goat anti-rabbit HRP which were diluted 1:1,000 in block.

Primary motor neuron imaging and neurite transport analysis

Primary motor neurons were cultured from flies as indicated above. At 4 days post-harvest, live primary motor neurons were imaged using an Olympus FV3000 scanning

confocal microscope with a 100x (NA 1.4) objective. For soma imaging, images were digitally zoomed to 2.95x for optimal resolution and a z-stack was obtained with 0.39μm slices through the entire soma. Images were presented as Z-projections which were made using Fiji/ImageJ.

For neurite transport movies, live cells were imaged with the 100x objective digitally zoomed to 1.79x so most branching neurites were imaged. Movies were collected containing four 0.39μm z-slices, over 100 frames (8:04 minutes). Movies were then analyzed using the Kymolyzer plugin in FIJI/ImageJ from which granule velocities and directionality were obtained, using a lower speed limit set to the pixel size, 0.138μm. (Basu et al., 2020).

To calculate the average number of neuritic granules in primary motor neurons, the max-intensity Z-projection of the first time point imaged was used (Frame 1). The Cell Counter plugin was used to manually count the number of granules within neurites for each of the movies used for tracking neuritic granules. Additionally, the proportion of neuritic granules 10μm or further from the cell body was determined from these images. The scale of these images was globally set and a symmetrical circle was drawn tightly around each cell using the oval selection tool in ImageJ, containing as much of the cell as possible. The diameter of each cell body was recorded in μm. The center of each circle was determined and marked using the Pencil tool. From this point, a line was drawn to the center of each granule within neurites and crude distance from the cell body was recorded in μm. The distances recorded were subtracted by the radius for their respective cell body to obtain the final distance used in analysis. Data were recorded in Excel and statistical analyses were performed in Prism.

Luciferase reporter assays

For a single well in a 24 well plate, 0.025 µg of the *firefly* luciferase (FLuc) 3' UTR mRNA reporter plasmid, 0.1 µg of the *Renilla* luciferase (RLuc) transfection control plasmid, and 0.25 µg of either the pAc5.1 /pAc5.1-λN vector or the pAc5.1:FMRP/pAc5.1-λN:FMRP mutant vectors were transfected. At three days post transfection, cells were thoroughly scraped and resuspended and 75 µL of cells were added in three technical replicates to a 96-well white, flat bottom polystyrene assay plate (Costar). Following the Dual-Glo Luciferase Assay System kit protocol (Promega), an equal volume of Dual-Glo Reagent and then Dual-Glo Stop & Glo Reagent were added to each well and incubated for 15 minutes before measuring FLuc and RLuc luminescence, respectively. Luminescence was measured using a Synergy™ HTX Multi-Mode Microplate Reader (BioTek).

Single molecule FISH and FISH-quant image analysis

Primary motor neurons were cultured from flies driving expression of *UAS-EGFP:FMRP, FMRΔ50* under the control of the *C380,cha-Gal80* driver as described above. Custom Stellaris® FISH Probes were designed against *Drosophila melanogaster camkii* and *chic* by utilizing the Stellaris® FISH Probe Designer (Biosearch Technologies Inc., Petaluma, CA) available online at www.biosearchtech.com/stellarisdesigner. Primary motor neurons were hybridized with the indicated Stellaris FISH Probe set labeled with either Quasar-570 or 670 (Biosearch Technologies, Inc.) following the manufacturer's instructions available online at

www.biosearchtech.com/stellarisprotocols. Essentially, at 3-4 days post culturing, cells growing on #1.5 cover glass were washed in 1X PBS (pH 7.4). Cells were then incubated in fixation buffer (3.7% formaldehyde in 1X PBS) for 10 minutes at room temperature, then washed twice in PBS. To permeabilize cells were immersed in 70% ethanol at 4°C for at least 1 hour and up to a week. Ethanol was aspirated and cells were washed in Stellaris Wash Buffer A for 5 minutes, then hybridized with the indicated probe(s) in a dark, humid hybridization chamber at 37°C for 5-16 hours. Probes were used at a final molarity of 0.125μM in Stellaris Hybridization buffer. Hybridization buffer was aspirated and cells were incubated with Wash Buffer A twice at 37°C for 30 minutes, then washed with Stellaris Wash Buffer B for 5 minutes at room temperature. Buffer was aspirated and Vectashield Mounting Medium was added to the #1.5 cover glass in the imaging dish and a clean coverslip was placed on top and sealed with clear nail polish. Imaging dishes were stored in the dark at -20°C for up to 2 days before imaging on an ONI Nanoimager S.

Approximately 15 cells were imaged per genotype using the widefield microscopy application on the ONI Nanoimager S for imaging smFISH probes. In order to detect smFISH probes, cells were exposed to 7% 570- or 640-laser power for 1,500 milliseconds. Z-projection was obtained with 0.2 μm slices through the entire cell. EGFP-FMRP was imaged sequentially which allowed us to distinguish the soma and neurites from background.

To analyze smFISH images, we used the FISH-Quant Matlab application to detect, localize and quantify mRNA in primary motor neurons (Mueller et al., 2013). Motor neuron soma and neurites were outlined individually, which allowed us to differentiate mRNAs

residing within the soma and neurites. Data were compiled in Excel and statistical analyses were performed in Prism.

Quantification and statistical analysis

All data were initially recorded in Excel (Microsoft) and then graphed and analyzed in Prism version 9.0.2 (GraphPad). Results were considered statistically significant if $p < 0.05$. Error bars throughout the study indicate mean ± SEM. n.s. = not significant, * $p < 0.05$, ** $p < 0.01$, *** $p < 0.001$, and **** $p < 0.0001$. Outliers were identified and removed using ROUT method in Prism, where necessary. Statistical tests and sample sizes for each experiment are indicated within the corresponding figure legend and/or in methods section.

FIGURE LEGENDS

Figure 1: The KH domains are differentially required to regulate FMRP granule formation in *Drosophila* S2R+ cells

(A) Schematic representation of *FMRP* variants used in this study. Arrowheads indicate where analogous FXS-causing point mutations were made in *dFMRP*. Deletion of the KH1 and KH2 domains is annotated with a break in FMRP sequence. (B) Western blot analysis of EGFP (GFP), FMRP, and α-tubulin protein levels in transfected cells. α-tubulin was used as a loading control (*= 100 kDa, **= 90 kDa, ***= 30 kDa, ****= 80 kDa, *****= 60 kDa). (C) Representative images of cells transiently transfected with the indicated GFP-tagged FMRP constructs. Scale bar = 2 μm. (D) Percentage of transfected cells forming GFP-FMRP granules. Data are presented as mean ± S.E. (approximately 100 cells per three experiments; one-way ANOVA, ****p<0.0001; **p<0.01). (E) Quantification of the number of granules within a cell, which was normalized to cell area in μm^2 (mean ± SE; n=15 cells each; Brown-Forsyth test; ****p<0.0001; ***p<0.001). (F) Quantification of the two major morphological phenotypes observed (n=100 cells each).

Figure 2: FXS-causing point mutants alter FMRP granule dynamics in S2R+ cells

(A) Representative time-lapse FRAP images of FMRP-mutants pre- and post-bleaching. Scale bar in whole cell image = 5μm. Scale bar in zoomed-in granule image = 0.5μm. (B) Fluorescence recovery curves of FMRP-mutants over 120 seconds. Data points are mean ± SE. (C) Mobile fraction of FMRP mutant granules (mean ± SE; Brown-Forsyth test; ***p<0.001). a.u.=arbitrary units. (D) Quantification of the average time in $\log_{10}$(seconds), for granules to recover to half their final intensity ($t_{1/2}$). For B, C, and D n=17-21 granules.

Figure 3: FXS-causing mutations alter SG dynamics and PB association

Representative images of the localization of S2R+ cells transfected with GFP-FMRP mutants (green) and Rin-mCherry (magenta) that are either not treated (A) or treated (B) with 0.5mM sodium arsenite for 45 minutes. Scale bars = 2μm. (C) Representative images of the localization of transiently transfected GFP-FMRP mutants immunostained against GFP (green) and HPat (magenta). Scale bar = 2μm. Percent of unstressed (D) or arsenite stressed (E) transfected cells forming Rin-positive SGs with or without 10% 1,6-HD treatment. Cells were incubated with 1,6-HD or with media (no treatment) for 20 minutes. Comparisons are made to WT-FMRP in each subcategory (mean ± SE; ~100 cells in triplicate; one-way ANOVA). (F) Average Pearson's correlation coefficient between FMRP-mutants and the stress granule marker, Rin, in arsenite treated cells (mean ± SE of 8-10 cells; Brown-Forsyth test). Percentage of unstressed (G) or arsenite stressed (H) transfected cells forming FMRP granules with or without 10% 1,6-HD compared to WT-FMRP (mean ± SE; ~100 cells in triplicate; one-way ANOVA). (I) Average Pearson's correlation coefficient between FMRP-mutants and HPat (mean ± SE of 12-13 cells; one-way ANOVA). In all graphs: * p<0.05, **p<0.01, ***p<0.001, ****p<0.0001.

Figure 4: FXS-causing mutations in FMRP disrupt NG formation and trafficking in primary MNs

(A) Representative Z-projections of major granule phenotype in *C380-Gal4, chagal80 Drosophila* primary motor neuron cell bodies. Scale bar = 2μm. (B) Percent of GFP-expressing motor neurons forming FMRP granules in the FMR1Δ50/+ background. Average is shown above respective bar (mean ± SE; 20 cells per triplicate, one-way

ANOVA). (C) Western blot analysis of EGFP (top), FMRP (middle), and α-tubulin (bottom) expression under the *C380-Gal4, cha-gal80* selective motor neuron driver in the larval CNS. α-tubulin was used as a loading control. (D) Representative images of WT and KH2* FMR1Δ50/+ primary MNs. Scale bar = 10μm. (E) Quantification of the average number of NGs within neurites of primary MNs (mean ± SE; 17-18 MNs, unpaired t test). (F) Percentage of neuritic granules that are distal ($\geq$10 μm) from the MN cell body (mean ± SE; 17-18 MNs, unpaired t test). Pie charts representing the fraction of neuritic granules that remain stationary (static/oscillatory) or move in the anterograde or retrograde direction (relative to the cell body) in WT (G) or KH2* (H) primary MNs. Percentages are annotated in the legend for each chart (n= total granules in 17 MNs). (I) Time-lapse images and kymographs illustrating NG movements within neurites of WT (left panel) and KH2* (right panel) NGs. Images are oriented with the cell body on the left. Each granule is annotated with a colored arrowhead which corresponds with the traces in the kymograph. Scale bar = 2 μm. (J) Comparison of anterograde and retrograde velocities of motile WT and KH2* neuritic NGs (mean ± SE; 46-75 granules per category; two-way ANOVA). (K) Average total displacement (μm) of all motile WT and KH2* NGs (mean ± SE; unpaired t test). In all graphs: * p<0.05, **p<0.01, ***p<0.001, ****p<0.0001.

Figure 5: FXS-causing mutations in FMRP disrupt NG dynamics in primary MNs

(A) Representative FRAP time lapse images of somatic NGs pre- and post-bleaching event. Scale bar in whole cell images = 2 μm. Scale bar in zoomed-in granule images = 1 μm. (B) Fluorescence recovery curves of somatic NGs over 200 seconds (mean ± SE; n $\geq$ 9 granules). (C) Representative FRAP time-lapse images of neuritic NGs pre- and

post-bleaching event. Neurites are outlined in green in the pre-bleach image, arrow heads point to the bleached granule. Scale bar = 1μm. (D) Fluorescence recovery curves of neuritic NGs showing fluorescence intensity relative to the initial pre-bleach intensity over 200 seconds (mean ± SE; n $\geq$ 13 granules). (E) Quantification of the average mobile fractions of somatic (left) or neuritic (right) mobile fraction of WT and KH2* NGs. a.u.=arbitrary units; p < 0.0001. (F) Quantification of the fluorescence half-time ($t_{1/2}$) of somatic or neuritic WT and KH2* NGs in seconds. For E and F n $\geq$ 9 granules.

Figure 6: FXS-causing mutations in FMRP affect FMRP function in translation and RNA transport

(A) Diagram of the FLuc reporters used in this study fused to the SV40 3'UTR containing the 5xBoxB sequence or the 3'UTR's of certain known targets of FMRP. Luciferase assays of (B) λN:HA-tethered FMRP-mutants repression of the 5xBoxB FLuc reporter or the untethered FMRP-mutants repression of FLuc fused with (C) *pickpocket* (*ppk*), (D) *fmr1*, (E) *chickadee (chic)* or (F) *camkii* 3'UTR. FLuc/RLuc ratios were normalized to empty vector ratios. Graph shows repression of the FLuc reporter by empty vector or FXS-causing point mutants compared to *pAc5.1-λNHA:FMRP (B) or pAc5.1-FMRP (C-F)* (mean ± SE; one-way ANOVA). Representative images of *camkii* (G) or *chic* (H) mRNA smFISH in primary MNs. Yellow arrowheads in images are distinguishing transcripts out in neurites. Scale bars = 10μm. Quantification of the average number of *camkii* (I) or *chic* (J) transcripts in neurites of each of the FMRP mutants (mean ± SE of 11-25 MNs; unpaired t test). In all graphs: * p<0.05, **p<0.01, ***p<0.001, ****p<0.0001.

AUTHOR CONTRIBUTIONS:

Designed experiments: ELS, SAB. Performed experiments: ELS

Analyzed the data: ELS, SAB. Wrote the paper: ELS, SAB

DECLARATION OF INTERESTS:

The authors declare no competing interests.

REFERENCES:

Agulhon, C., Blanchet, P., Kobetz, A., Marchant, D., Faucon, N., Sarda, P., Moraine, C., Sittler, A., Biancalana, V., Malafosse, A.*, et al.* (1999). Expression of FMR1, FXR1, and FXR2 genes in human prenatal tissues. J Neuropathol Exp Neurol *58*, 867-880.

Akins, M.R., Leblanc, H.F., Stackpole, E.E., Chyung, E., and Fallon, J.R. (2012). Systematic mapping of fragile X granules in the mouse brain reveals a potential role for presynaptic FMRP in sensorimotor functions. J Comp Neurol *520*, 3687-3706.

Alberti, S. (2017). Phase separation in biology. Curr Biol *27*, R1097-R1102.

Antar, L.N., Afroz, R., Dictenberg, J.B., Carroll, R.C., and Bassell, G.J. (2004). Metabotropic glutamate receptor activation regulates Fragile X mental retardation protein and Fmr1 mRNA localization differentially in dendrites and at synapses. J Neurosci *24*, 2648-2655.

Antar, L.N., Dictenberg, J.B., Plociniak, M., Afroz, R., and Bassell, G.J. (2005). Localization of FMRP-associated mRNA granules and requirement of microtubules for activity-dependent trafficking in hippocampal neurons. Genes Brain Behav *4*, 350-359.

Antar, L.N., Li, C., Zhang, H., Carroll, R.C., and Bassell, G.J. (2006). Local functions for FMRP in axon growth cone motility and activity-dependent regulation of filopodia and spine synapses. Mol Cell Neurosci *32*, 37-48.

Ascano, M., Jr., Mukherjee, N., Bandaru, P., Miller, J.B., Nusbaum, J.D., Corcoran, D.L., Langlois, C., Munschauer, M., Dewell, S., Hafner, M., *et al.* (2012). FMRP targets distinct mRNA sequence elements to regulate protein expression. Nature *492*, 382-386.

Athar, Y.M., and Joseph, S. (2020). RNA-Binding Specificity of the Human Fragile X Mental Retardation Protein. J Mol Biol *432*, 3851-3868.

Banani, S.F., Lee, H.O., Hyman, A.A., and Rosen, M.K. (2017). Biomolecular condensates: organizers of cellular biochemistry. Nat Rev Mol Cell Biol *18*, 285-298.

Banani, S.F., Rice, A.M., Peeples, W.B., Lin, Y., Jain, S., Parker, R., and Rosen, M.K. (2016). Compositional Control of Phase-Separated Cellular Bodies. Cell *166*, 651-663.

Barbee, S.A., Estes, P.S., Cziko, A.M., Hillebrand, J., Luedeman, R.A., Coller, J.M., Johnson, N., Howlett, I.C., Geng, C., Ueda, R., *et al.* (2006). Staufen- and FMRP-containing neuronal RNPs are structurally and functionally related to somatic P bodies. Neuron *52*, 997-1009.

Chae, Y.S., Lee, S.H., Cheang, Y.H., Lee, N., Rim, Y.S., Jang, D.J., and Kaang, B.K. (2010). Neuronal RNA granule contains ApCPEB1, a novel cytoplasmic polyadenylation element binding protein, in Aplysia sensory neuron. Exp Mol Med *42*, 30-37.

Chen, E., Sharma, M.R., Shi, X., Agrawal, R.K., and Joseph, S. (2014). Fragile X mental retardation protein regulates translation by binding directly to the ribosome. Mol Cell *54*, 407-417.

Christie, S.B., Akins, M.R., Schwob, J.E., and Fallon, J.R. (2009). The FXG: a presynaptic fragile X granule expressed in a subset of developing brain circuits. J Neurosci *29*, 1514-1524.

Chyung, E., LeBlanc, H.F., Fallon, J.R., and Akins, M.R. (2018). Fragile X granules are a family of axonal ribonucleoprotein particles with circuit-dependent protein composition and mRNA cargos. J Comp Neurol *526*, 96-108.

Coller, J., and Parker, R. (2005). General translational repression by activators of mRNA decapping. Cell *122*, 875-886.

Cougot, N., Bhattacharyya, S.N., Tapia-Arancibia, L., Bordonne, R., Filipowicz, W., Bertrand, E., and Rage, F. (2008). Dendrites of mammalian neurons contain specialized P-body-like structures that respond to neuronal activation. J Neurosci *28*, 13793-13804.

Darnell, J.C., Fraser, C.E., Mostovetsky, O., Stefani, G., Jones, T.A., Eddy, S.R., and Darnell, R.B. (2005). Kissing complex RNAs mediate interaction between the Fragile-X mental retardation protein KH2 domain and brain polyribosomes. Genes Dev *19*, 903-918.

Davidovic, L., Jaglin, X.H., Lepagnol-Bestel, A.M., Tremblay, S., Simonneau, M., Bardoni, B., and Khandjian, E.W. (2007). The fragile X mental retardation protein is a molecular adaptor between the neurospecific KIF3C kinesin and dendritic RNA granules. Hum Mol Genet *16*, 3047-3058.

De Boulle, K., Verkerk, A.J., Reyniers, E., Vits, L., Hendrickx, J., Van Roy, B., Van den Bos, F., de Graaff, E., Oostra, B.A., and Willems, P.J. (1993). A point mutation in the FMR-1 gene associated with fragile X mental retardation. Nat Genet *3*, 31-35.

Dictenberg, J.B., Swanger, S.A., Antar, L.N., Singer, R.H., and Bassell, G.J. (2008). A direct role for FMRP in activity-dependent dendritic mRNA transport links filopodial-spine morphogenesis to fragile X syndrome. Dev Cell *14*, 926-939.

Drozd, M., Bardoni, B., and Capovilla, M. (2018). Modeling Fragile X Syndrome in Drosophila. Front Mol Neurosci *11*, 124.

El Fatimy, R., Davidovic, L., Tremblay, S., Jaglin, X., Dury, A., Robert, C., De Koninck, P., and Khandjian, E.W. (2016). Tracking the Fragile X Mental Retardation Protein in a Highly Ordered Neuronal RiboNucleoParticles Population: A Link between Stalled Polyribosomes and RNA Granules. Plos Genet *12*, e1006192.

Estes, P.S., O'Shea, M., Clasen, S., and Zarnescu, D.C. (2008). Fragile X protein controls the efficacy of mRNA transport in Drosophila neurons. Mol Cell Neurosci *39*, 170-179.

Feng, Y., Absher, D., Eberhart, D.E., Brown, V., Malter, H.E., and Warren, S.T. (1997). FMRP associates with polyribosomes as an mRNP, and the I304N mutation of severe fragile X syndrome abolishes this association. Mol Cell *1*, 109-118.

Formicola, N., Vijayakumar, J., and Besse, F. (2019). Neuronal ribonucleoprotein granules: Dynamic sensors of localized signals. Traffic *20*, 639-649.

Gareau, C., Houssin, E., Martel, D., Coudert, L., Mellaoui, S., Huot, M.E., Laprise, P., and Mazroui, R. (2013a). Characterization of fragile X mental retardation protein recruitment and dynamics in Drosophila stress granules. PLoS One *8*, e55342.

Gareau, C., Martel, D., Coudert, L., Mellaoui, S., and Mazroui, R. (2013b). Characterization of Fragile X Mental Retardation Protein granules formation and dynamics in Drosophila. Biol Open *2*, 68-81.

Gopal, P.P., Nirschl, J.J., Klinman, E., and Holzbaur, E.L. (2017). Amyotrophic lateral sclerosis-linked mutations increase the viscosity of liquid-like TDP-43 RNP granules in neurons. Proc Natl Acad Sci U S A *114*, E2466-E2475.

Jain, S., Wheeler, J.R., Walters, R.W., Agrawal, A., Barsic, A., and Parker, R. (2016). ATPase-Modulated Stress Granules Contain a Diverse Proteome and Substructure. Cell *164*, 487-498.

Kim, S.H., Dong, W.K., Weiler, I.J., and Greenough, W.T. (2006). Fragile X mental retardation protein shifts between polyribosomes and stress granules after neuronal injury by arsenite stress or in vivo hippocampal electrode insertion. J Neurosci *26*, 2413-2418.

Kim, T.H., Tsang, B., Vernon, R.M., Sonenberg, N., Kay, L.E., and Forman-Kay, J.D. (2019). Phospho-dependent phase separation of FMRP and CAPRIN1 recapitulates regulation of translation and deadenylation. Science *365*, 825-829.

Kroschwald, S., Maharana, S., and Alberti, S. (2017). Hexanediol: a chemical probe to investigate the material properties of membrane-less compartments. Matters.

Lai, A., Valdez-Sinon, A.N., and Bassell, G.J. (2020). Regulation of RNA granules by FMRP and implications for neurological diseases. Traffic *21*, 454-462.

Li, C., Bassell, G.J., and Sasaki, Y. (2009). Fragile X Mental Retardation Protein is Involved in Protein Synthesis-Dependent Collapse of Growth Cones Induced by Semaphorin-3A. Front Neural Circuits *3*, 11.

Li, P., Banjade, S., Cheng, H.C., Kim, S., Chen, B., Guo, L., Llaguno, M., Hollingsworth, J.V., King, D.S., Banani, S.F.*, et al.* (2012). Phase transitions in the assembly of multivalent signalling proteins. Nature *483*, 336-340.

Martin, E.W., and Holehouse, A.S. (2020). Intrinsically disordered protein regions and phase separation: sequence determinants of assembly or lack thereof. Emerg Top Life Sci *4*, 307-329.

Mittag, T., and Parker, R. (2018). Multiple Modes of Protein-Protein Interactions Promote RNP Granule Assembly. J Mol Biol *430*, 4636-4649.

Molliex, A., Temirov, J., Lee, J., Coughlin, M., Kanagaraj, A.P., Kim, H.J., Mittag, T., and Taylor, J.P. (2015). Phase separation by low complexity domains promotes stress granule assembly and drives pathological fibrillization. Cell *163*, 123-133.

Morales, J., Hiesinger, P.R., Schroeder, A.J., Kume, K., Verstreken, P., Jackson, F.R., Nelson, D.L., and Hassan, B.A. (2002). Drosophila fragile X protein, DFXR, regulates neuronal morphology and function in the brain. Neuron *34*, 961-972.

Myrick, L.K., Deng, P.Y., Hashimoto, H., Oh, Y.M., Cho, Y., Poidevin, M.J., Suhl, J.A., Visootsak, J., Cavalli, V., Jin, P.*, et al.* (2015a). Independent role for presynaptic FMRP revealed by an FMR1 missense mutation associated with intellectual disability and seizures. Proc Natl Acad Sci U S A *112*, 949-956.

Myrick, L.K., Hashimoto, H., Cheng, X., and Warren, S.T. (2015b). Human FMRP contains an integral tandem Agenet (Tudor) and KH motif in the amino terminal domain. Hum Mol Genet *24*, 1733-1740.

Myrick, L.K., Nakamoto-Kinoshita, M., Lindor, N.M., Kirmani, S., Cheng, X., and Warren, S.T. (2014). Fragile X syndrome due to a missense mutation. Eur J Hum Genet *22*, 1185-1189.

Patel, A., Lee, H.O., Jawerth, L., Maharana, S., Jahnel, M., Hein, M.Y., Stoynov, S., Mahamid, J., Saha, S., Franzmann, T.M.*, et al.* (2015). A Liquid-to-Solid Phase Transition of the ALS Protein FUS Accelerated by Disease Mutation. Cell *162*, 1066-1077.

Pieretti, M., Zhang, F.P., Fu, Y.H., Warren, S.T., Oostra, B.A., Caskey, C.T., and Nelson, D.L. (1991). Absence of expression of the FMR-1 gene in fragile X syndrome. Cell *66*, 817-822.

Pradhan, S.J., Nesler, K.R., Rosen, S.F., Kato, Y., Nakamura, A., Ramaswami, M., and Barbee, S.A. (2012). The conserved P body component HPat/Pat1 negatively regulates synaptic terminal growth at the larval Drosophila neuromuscular junction. J Cell Sci *125*, 6105-6116.

Prieto, M., Folci, A., Poupon, G., Schiavi, S., Buzzelli, V., Pronot, M., Francois, U., Pousinha, P., Lattuada, N., Abelanet, S.*, et al.* (2021). Missense mutation of Fmr1 results in impaired AMPAR-mediated plasticity and socio-cognitive deficits in mice. Nat Commun *12*, 1557.

Ray, D., Kazan, H., Cook, K.B., Weirauch, M.T., Najafabadi, H.S., Li, X., Gueroussov, S., Albu, M., Zheng, H., Yang, A.*, et al.* (2013). A compendium of RNA-binding motifs for decoding gene regulation. Nature *499*, 172-177.

Reeve, S.P., Bassetto, L., Genova, G.K., Kleyner, Y., Leyssen, M., Jackson, F.R., and Hassan, B.A. (2005). The Drosophila fragile X mental retardation protein controls actin dynamics by directly regulating profilin in the brain. Curr Biol *15*, 1156-1163.

Rehwinkel, J., Behm-Ansmant, I., Gatfield, D., and Izaurralde, E. (2005). A crucial role for GW182 and the DCP1:DCP2 decapping complex in miRNA-mediated gene silencing. RNA *11*, 1640-1647.

Richter, J.D., and Zhao, X. (2021). The molecular biology of FMRP: new insights into fragile X syndrome. Nat Rev Neurosci.

Santoro, M.R., Bray, S.M., and Warren, S.T. (2012). Molecular mechanisms of fragile X syndrome: a twenty-year perspective. Annu Rev Pathol *7*, 219-245.

Schuman, E.M., Dynes, J.L., and Steward, O. (2006). Synaptic regulation of translation of dendritic mRNAs. J Neurosci *26*, 7143-7146.

Schwartz, J.C., Wang, X., Podell, E.R., and Cech, T.R. (2013). RNA seeds higher-order assembly of FUS protein. Cell Rep *5*, 918-925.

Shin, Y., and Brangwynne, C.P. (2017). Liquid phase condensation in cell physiology and disease. Science *357*.

Sudhakaran, I.P., Hillebrand, J., Dervan, A., Das, S., Holohan, E.E., Hulsmeier, J., Sarov, M., Parker, R., VijayRaghavan, K., and Ramaswami, M. (2014). FMRP and Ataxin-2 function together in long-term olfactory habituation and neuronal translational control. Proc Natl Acad Sci U S A *111*, E99-E108.

Suhl, J.A., Chopra, P., Anderson, B.R., Bassell, G.J., and Warren, S.T. (2014). Analysis of FMRP mRNA target datasets reveals highly associated mRNAs mediated by G-quadruplex structures formed via clustered WGGA sequences. Hum Mol Genet *23*, 5479-5491.

Suhl, J.A., and Warren, S.T. (2015). Single-Nucleotide Mutations in FMR1 Reveal Novel Functions and Regulatory Mechanisms of the Fragile X Syndrome Protein FMRP. J Exp Neurosci *9*, 35-41.

Tourriere, H., Chebli, K., Zekri, L., Courselaud, B., Blanchard, J.M., Bertrand, E., and Tazi, J. (2003). The RasGAP-associated endoribonuclease G3BP assembles stress granules. J Cell Biol *160*, 823-831.

Tsang, B., Arsenault, J., Vernon, R.M., Lin, H., Sonenberg, N., Wang, L.Y., Bah, A., and Forman-Kay, J.D. (2019). Phosphoregulated FMRP phase separation models activity-

dependent translation through bidirectional control of mRNA granule formation. Proc Natl Acad Sci U S A *116*, 4218-4227.

Valverde, R., Pozdnyakova, I., Kajander, T., Venkatraman, J., and Regan, L. (2007). Fragile X mental retardation syndrome: structure of the KH1-KH2 domains of fragile X mental retardation protein. Structure *15*, 1090-1098.

Van Treeck, B., and Parker, R. (2018). Emerging Roles for Intermolecular RNA-RNA Interactions in RNP Assemblies. Cell *174*, 791-802.

Vijayakumar, J., Perrois, C., Heim, M., Bousset, L., Alberti, S., and Besse, F. (2019). The prion-like domain of Drosophila Imp promotes axonal transport of RNP granules in vivo. Nat Commun *10*, 2593.

Wan, L., Dockendorff, T.C., Jongens, T.A., and Dreyfuss, G. (2000). Characterization of dFMR1, a Drosophila melanogaster homolog of the fragile X mental retardation protein. Mol Cell Biol *20*, 8536-8547.

Xu, K., Bogert, B.A., Li, W., Su, K., Lee, A., and Gao, F.B. (2004). The fragile X-related gene affects the crawling behavior of Drosophila larvae by regulating the mRNA level of the DEG/ENaC protein pickpocket1. Curr Biol *14*, 1025-1034.

Zang, J.B., Nosyreva, E.D., Spencer, C.M., Volk, L.J., Musunuru, K., Zhong, R., Stone, E.F., Yuva-Paylor, L.A., Huber, K.M., Paylor, R.*, et al.* (2009). A mouse model of the human Fragile X syndrome I304N mutation. Plos Genet *5*, e1000758.

Zhang, Y., O'Connor, J.P., Siomi, M.C., Srinivasan, S., Dutra, A., Nussbaum, R.L., and Dreyfuss, G. (1995). The fragile X mental retardation syndrome protein interacts with novel homologs FXR1 and FXR2. Embo J *14*, 5358-5366.

Zhang, Y.Q., Bailey, A.M., Matthies, H.J., Renden, R.B., Smith, M.A., Speese, S.D., Rubin, G.M., and Broadie, K. (2001). Drosophila fragile X-related gene regulates the MAP1B homolog Futsch to control synaptic structure and function. Cell *107*, 591-603.

Figure 1: The KH domains are differentially required to regulate FMRP granule formation

A.

B.

C.

D.

E.

F.
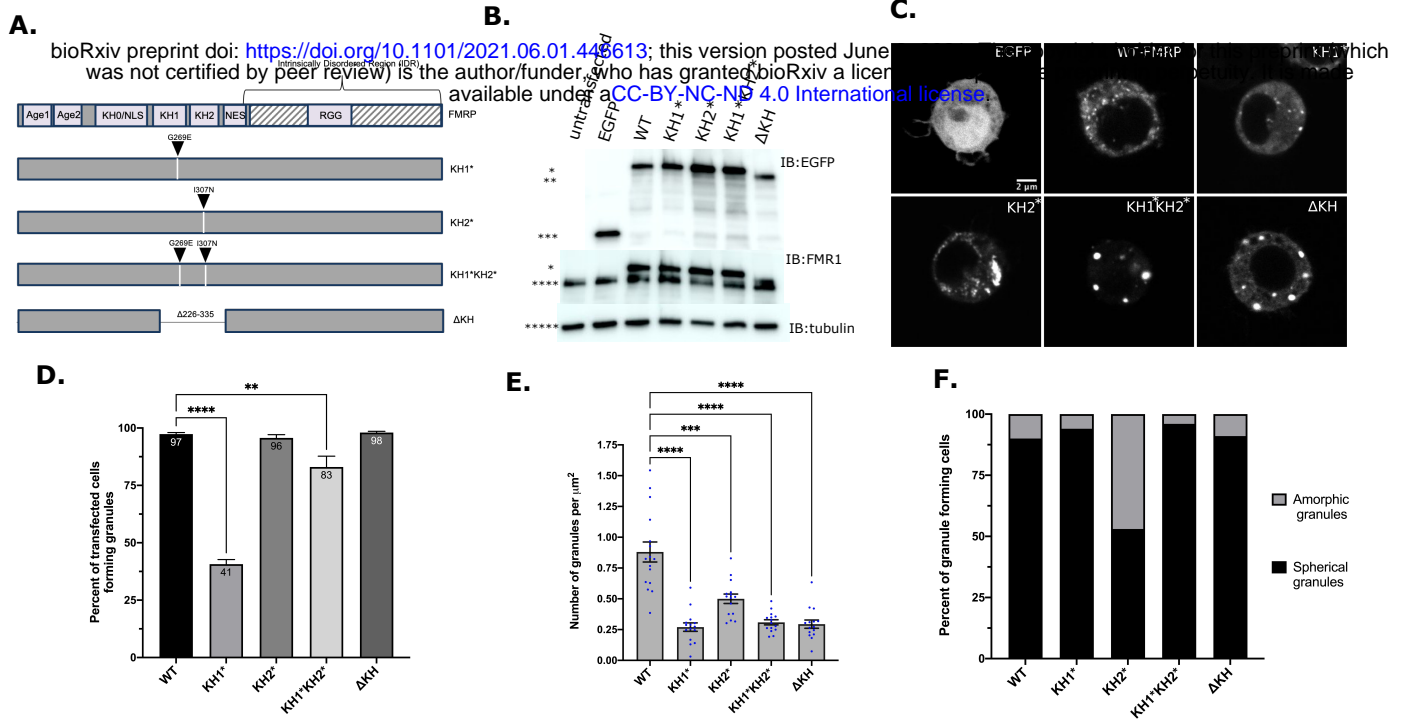
Figure 2: FXS-causing point mutants alter FMRP-granules dynamics in S2R+ cells
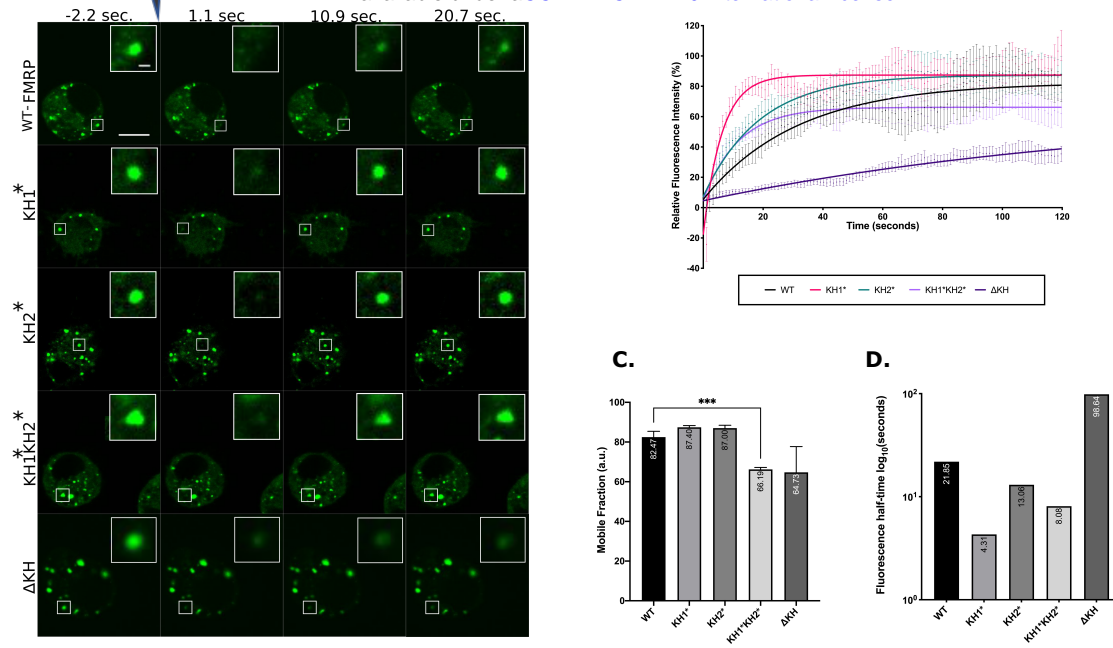
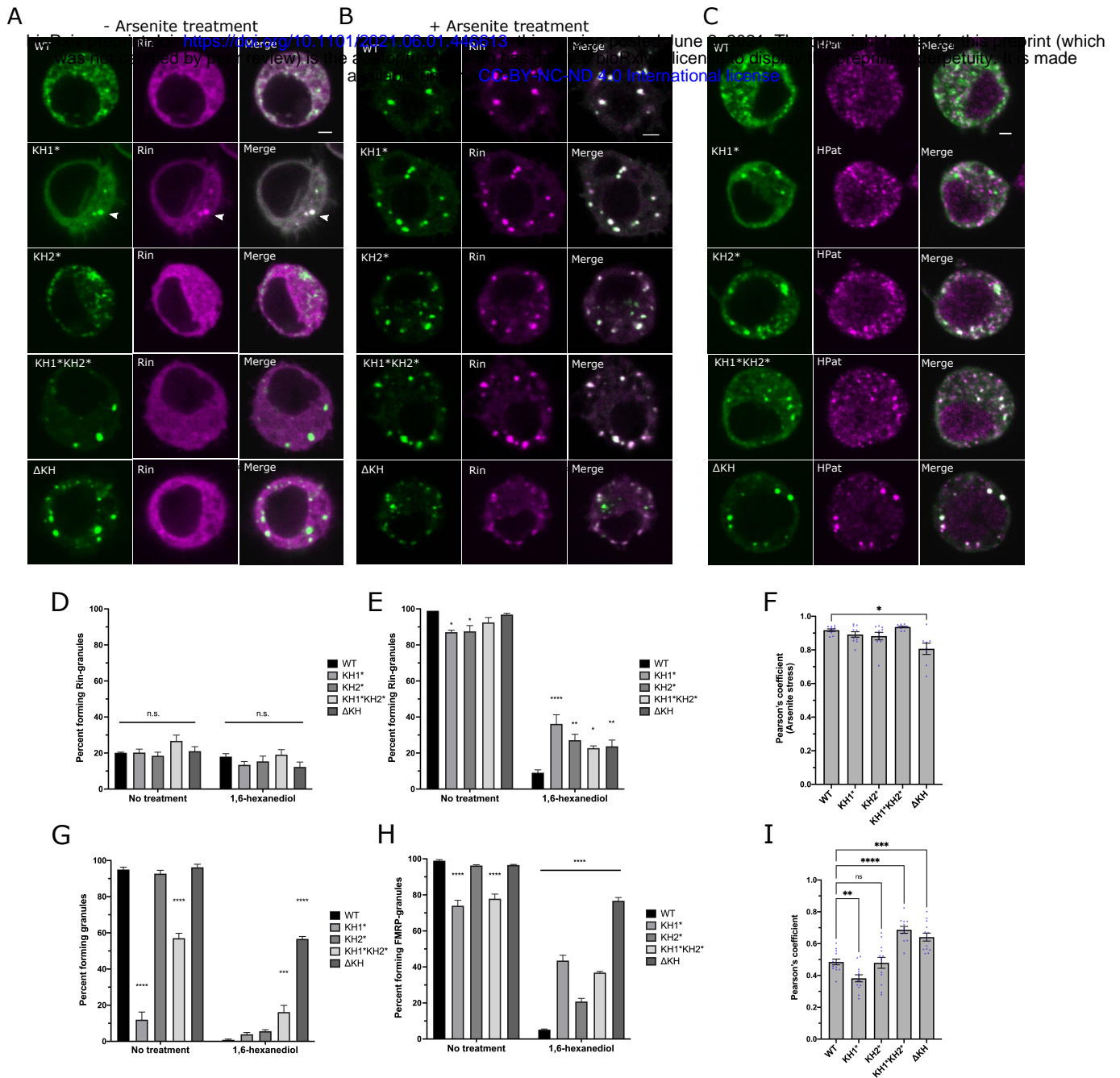# Figure 3: FXS-causing mutations alter stress granule dynamics and P-body association

Figure 4: FXS-causing mutations in FMRP disrupt NG formation and dynamics in primary MNs.
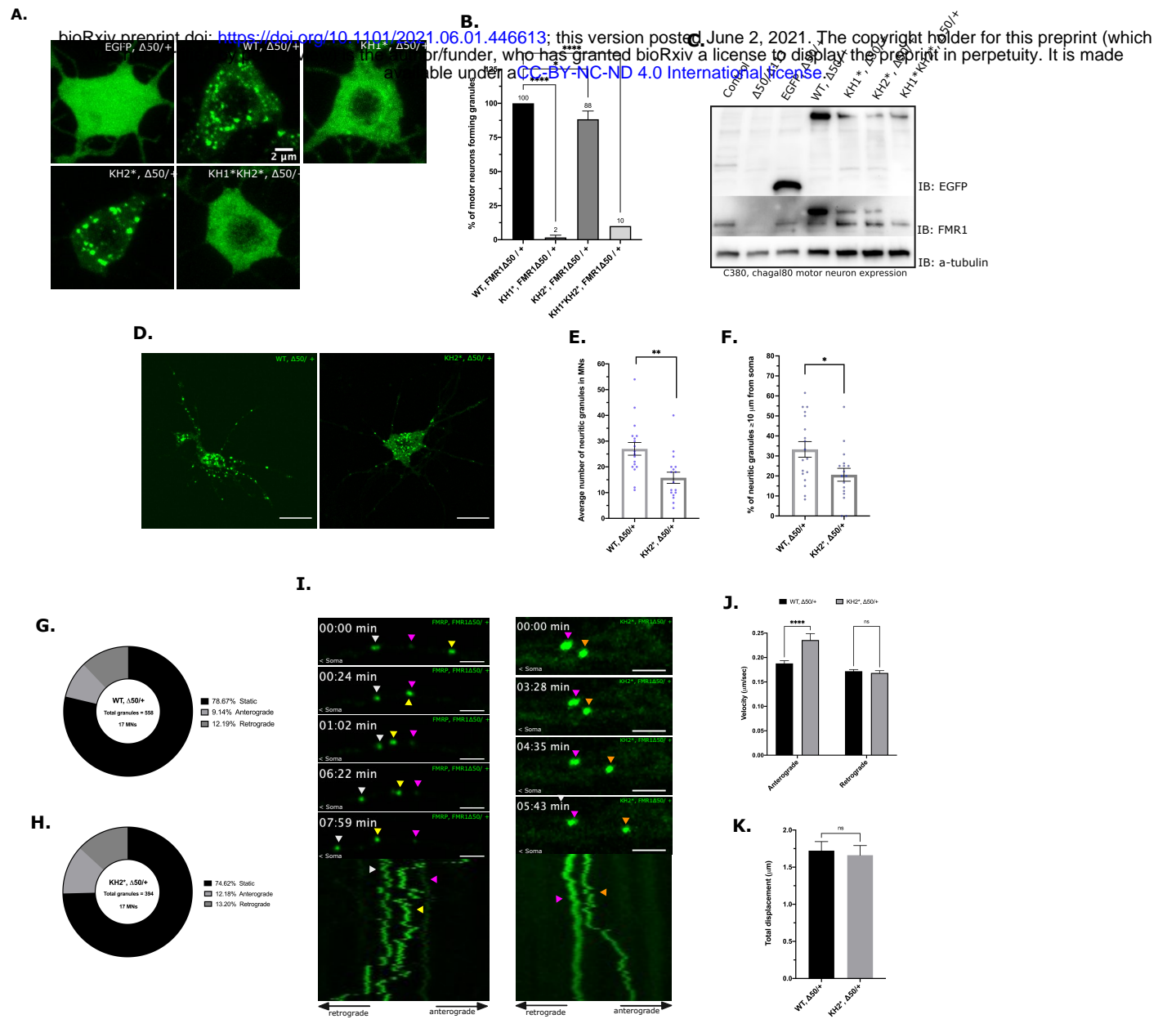
Figure 5: FXS-causing mutations in FMRP disrupt NG dynamics in primary MNs.
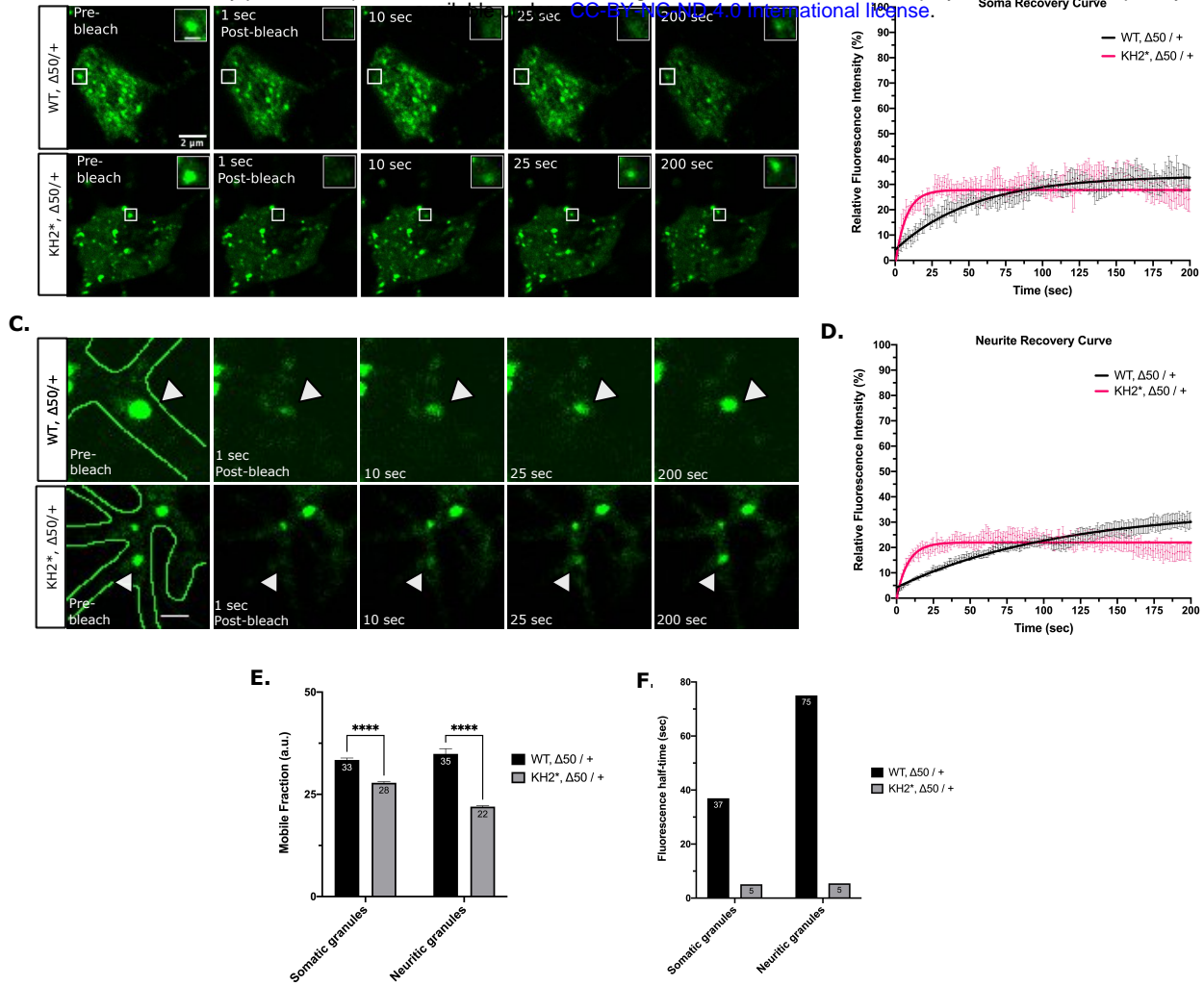
Figure 6: FXS-causing mutations in FMRP affect FMRP functinon in translation and transport